

Cathodic Modification, Numerical Simulation and Experimental Investigation on Electrochemical Machining for the Small Inner-walled Ring Groove

Changfu Zhang^{1,2,*}, Haihong Ai^{1,2}, Zhenghu Yan^{1,2}, Xinguang Jiang^{1,2}, Peiyong Cheng^{1,2}, Hao Tian^{1,2}, Yanwei Hu^{1,2}

¹ School of Mechatronics Engineering, Xi'an Technological University, Xi'an 710021, China

² Shaanxi Key Laboratory of Non-Traditional Machining, Xi'an 710021, China

*E-mail: cfzhang@xatu.edu.cn

Received: 11 October 2019 / Accepted: 9 December 2019 / Published: 10 March 2020

Some important magnetic conductors, pneumatic valves and hydraulic valves made of corrosion-resistant alloy Cr16Fe (1J116) are often applied in harsh environments. However, it is very challenging to machine the inner-walled ring grooves that broadly exist in these workpieces. Electrochemical machining (ECM) is regarded as an ideal manufacturing technology to machine this kind of structure without residual stress, metamorphic layers or microcracks. However, the inner-walled ring grooves machined with ECM with the typical cylindrical cathode are shaped like a little drum and are not flat at the bottom. In this paper, a working-surface curvature cathodic modification and numerical simulation method is proposed to solve this problem. First, the working surface of the cathode is modified into an inward curved surface and is used in the flow field simulation model in which the k- ϵ equation is employed. Then, the coupling analysis of the flow field and the electric field is carried out with COMSOL Multiphysics. The simulation results show that the machining quality of the inner-walled ring groove is improved with the modified cathode because the flow field distributions and the electric field distributions in the machining gap are more uniform than before. Finally, verification experiments with the modified cathode are conducted. The experimental results show that the machined inner-walled ring groove is of good quality, and the bottom of the groove is flat. The experimental results agree with the simulation results. This study is meaningful to provide a probable solution to improve the machining quality of the inner-walled structure workpieces without residual stress, metamorphic layers or microcracks.

Keywords: Electrochemical machining; Small inner-walled ring groove; Cathode modification; Numerical simulation; Experimental investigation

1. INTRODUCTION

Various magnetic conductors, pneumatic valves and hydraulic valves made of corrosion-

resistant alloy material Cr16Fe (1J116) are widely applied in harsh environments (e.g., the liquid rocket motor) because of the good properties of the alloy, such as high saturation magnetic induction, high Curie temperature and high corrosion resistance. The inner-walled groove is one of the typical structures of these workpieces. To machine this kind of structure, electrodischarge machining (EDM) is often employed at present, and a time-consuming polishing process is then used to remove the metamorphic layer produced during EDM. It is difficult to machine the inner-walled structures with traditional mechanical cutting technologies because of the residual stress, the poor tool reachability and the tool wear. Other technologies, such as laser machining, ultrasonic machining and some other nontraditional machining technologies, are also not ideal methods to machine the small inner-walled structures because deterioration layers, microcracks or residual stresses will be generated during machining. Thus, it is very challenging to machine the small inner-walled structures of 1J116 without residual stress, recast layers or microcracks.

Electrochemical machining (ECM) has become an attractive method because of its ability to machine parts without generating a defective surface layer [1]. ECM is an effective nontraditional machining technique to shape metals by controlling anodic dissolution without any contact between the tool and the workpiece [2]. ECM has been widely used in the fields of aeronautics, astronautics, defense and medical industries because of its outstanding advantages, such as the high removal rate, superior machinability without tool wear, good surface quality and capability to machine complex structural parts [3-6]. Additionally, the workpieces machined with ECM have smooth surfaces and do not need to be polished in further production steps [7-9]. Thus, ECM is gradually becoming an ideal manufacturing technology for the inner-walled structures.

Liu [10] used a cylindrical cathode to machine a kind of inner-walled structure, but the structure has an obvious drum shape. Mi [11] studied an ECM method to machine complex internal-feature holes by controlling the conductive area ratio with a conductive coil. However, the winding precision of the coil was not easily controlled. Recently, my research team applied disk-shaped cathodes to machine the inner-walled ring grooves of 1J116 and found that the machined grooves were not of good quality [12]. The bottoms of the machined grooves were drum-shaped and were not flat. From these studies, it can be concluded that the conventional cylindrical cathode results in an obvious drum shape at the bottom of the machined inner-walled ring grooves.

Cathode modification is important for improving the machining accuracy of ECM [13, 14]. Zhu [15] established a digital cathode modification model based on the improved back-propagation neural network and simulated it for the electrochemical machining of the blades of airplane engines. Xu [16] proposed a variable-gap amendment method to modify the cathode and built a mathematical model to improve the electrochemical machining accuracy of the blade.

In this paper, a working surface-curvature modification method for the cathode is proposed to reduce the drum-shape effect and to improve the machining quality of the inner-walled ring groove in ECM. The k - ε equation is used as the flow field model for simulation. Then, the coupling analyses of the flow field and the electric field are carried out using COMSOL Multiphysics. The surface profile of the inner-walled ring groove is predicted by simulation. Finally, a machining experiment is carried out to verify the effectiveness of the cathodic modification and numerical simulation method.

2. CATHODIC MODIFICATION AND NUMERICAL SIMULATION

Figure 1(a) shows the inner-walled ring groove machined with the conventional cylindrical cathode, the schematic diagram of which is shown in Figure 1(b). The bottom of the groove is not flat, and the middle section is drum-shaped because of obvious overcut. After careful analysis, the flow field distributions and electric field distributions of the machining gap are found to be not very good when the conventional cylindrical cathode is applied. To improve the machining quality of the small inner-walled ring groove, it is necessary and meaningful to study a cathodic modification and numerical simulation method.

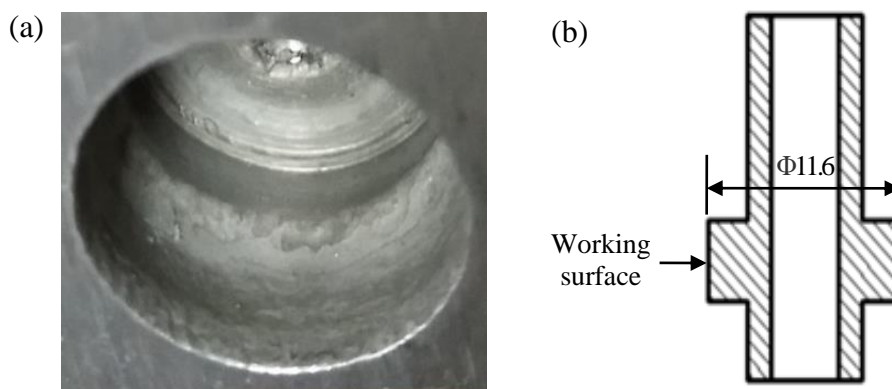


Figure 1. The machined groove and the cathode: (a) the machined inner-walled groove and (b) the schematic diagram of the conventional cylindrical cathode.

In this section, a working surface-curvature modification method for the cathode is proposed and the finite element method is applied to simulate the flow field and the electric field in the machining gap between the workpiece and the modified cathode. In this paper, COMSOL Multiphysics is employed to conduct the numerical simulation.

2.1 Cathodic modification and the geometrical model of the numerical simulation

To reduce the overcut and drum shape of the machined inner-walled groove, the shape of the working surface of the cathode needs to be modified. According to Faraday's Law, the dissolution rate of the groove is closely related to the current density, and the current density is directly affected by the machining gap between the workpiece and the cathode. Thus, increasing the machining gap in the middle section by modifying the working surface is expected to reduce the drum-shape of the groove. In this paper, the working surface of the cathode is modified into an inward curved surface with a small curvature radius.

To analyze the flow field and the electric field of the machining gap, the geometrical model for coupling analysis was built and shown in Figure 2. In this figure, the working surface of the cathode has been modified. In the model, workpiece material is corrosion-resistant 1J116, and the cathode material is copper. The machining gap between the workpiece and the cathode is 0.1 mm. The

electrolyte is a mixture solution of 10 wt % NaCl + 16 wt % NaNO₃ + 2 wt % NaClO₃, which showed good performance in the previous machining experiments.

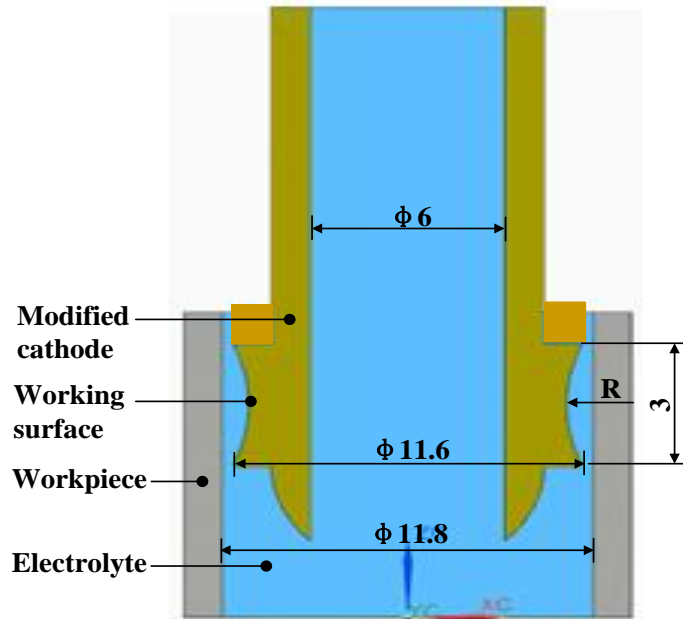


Figure 2. Geometric model.

2.2 The mathematical model

To simplify the flow field model, the following assumptions are made about the machining gap:

(a) The fluid is an incompressible and constant Newtonian fluid, and its dynamic viscosity does not change with the change in the velocity gradient.

(b) The electrolyte in the machining gap is always in a turbulent state to ensure the uniformity of the flow field distribution and to avoid the concentration polarization in ECM, and the temperature effect on ECM and energy-loss can be ignored.

$$\rho \frac{dV}{dt} = \rho g - \nabla P + \mu \nabla^2 V \tag{1}$$

$$\nabla \cdot V = \frac{\partial u}{\partial x} + \frac{\partial v}{\partial y} + \frac{\partial w}{\partial z} = 0 \tag{2}$$

where ρ is the electrolyte density (g/cm³), P is the electrolyte pressure (Pa), g is the gravitational acceleration (m/s²), μ is the component of the velocity vector in the x-direction (m/s), and ∇V is the volume expansion ratio (%).

In ECM, the flow state under a certain pressure is considered turbulent [17, 18]. The electrolyte flow satisfies the standard k-ε model in the simulation, and the equations are as follows:

$$\text{k-equation: } \frac{\partial k}{\partial t} + u_i \frac{\partial k}{\partial x_i} = \frac{\partial}{\partial x_i} \left[\left(C_k \frac{k^2}{\varepsilon} + \nu \right) \frac{\partial k}{\partial x_i} \right] + G_k - \varepsilon \tag{3}$$

$$\text{ε-equation: } \frac{\partial \varepsilon}{\partial t} + u_i \frac{\partial \varepsilon}{\partial x_i} = \frac{\partial}{\partial x_i} \left[\left(C_\varepsilon \frac{k^2}{\varepsilon} + \nu \right) \frac{\partial \varepsilon}{\partial x_i} \right] + \frac{C_{1\varepsilon}}{C_{2\varepsilon}} G_k - C_{2\varepsilon} \rho \frac{\varepsilon^2}{k} \tag{4}$$

$$\text{G}_k\text{-equation: } G_k = C_\mu \frac{k^2}{\varepsilon} \left(\frac{\partial u_i}{\partial x_i} + \frac{\partial u_j}{\partial x_i} \right) \frac{\partial u_i}{\partial x_j} \tag{5}$$

$$\text{Turbulent equation: } \frac{\partial(\rho k u_i)}{\partial x_i} = \frac{\partial}{\partial x_j} \left[\frac{\partial k}{\partial x_j} \left(\mu + \frac{\mu_i}{\sigma_k} \right) \right] + \mu_i \frac{\partial u_i}{\partial x_j} \left(\frac{\partial u_i}{\partial x_j} + \frac{\partial u_j}{\partial x_i} \right) - \rho \varepsilon \tag{6}$$

where k is the turbulent kinetic energy (J), ε is the dissipation rate (%), G_k is the turbulent energy caused by the average velocity gradient, C_u , $C_{1\varepsilon}$ and $C_{2\varepsilon}$ are the constants, ν is the dynamic viscosity coefficient ($\text{N}\cdot\text{s}/\text{m}^2$), ρ is the electrolyte density (g/cm^3), μ is the kinematic viscosity coefficient ($\text{Pa}\cdot\text{s}$), i equals 1, 2 and 3, and j equals 1, 2 and 3.

2.3 Boundary conditions

Coupling analyses of the flow field and the electric field are simulated with the turbulence model shown in Figure 3. To simplify the analysis, three assumptions [19] are made: the surface current density of the workpiece is determined by Ohm's effect; the conductivity of the electrolyte is equal everywhere; and the potential of the cathode surface is equal everywhere.

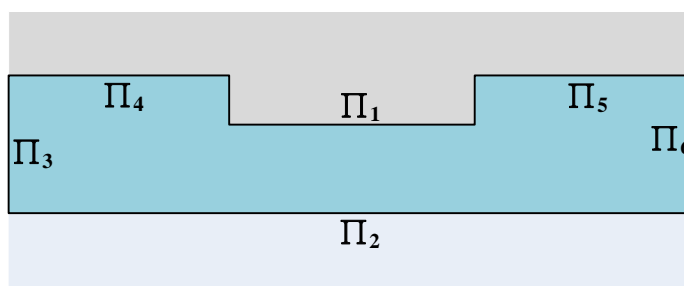


Figure 3. Physical model.

According to Laplace's equation, the electric potential distribution satisfies the following expression:

$$\nabla^2\varphi = 0 \tag{7}$$

where φ is the electric potential.

The boundary conditions are expressed as:

$$\begin{aligned} \varphi|_{\Pi_1} &= 0 \text{ (cathode boundary)} \\ \varphi|_{\Pi_{3,4,5,6}} &= 0 \text{ (free boundary)} \\ \varphi|_{\Pi_2} &\approx U \text{ (workpiece boundary)} \end{aligned}$$

The dissolution rate v of the workpiece is expressed as:

$$v = \eta\omega i \tag{8}$$

where i is the current density, ω is the electrochemical equivalent and η is the current efficiency.

The current density i is closely related with the electric potential φ :

$$i = k \frac{\partial\varphi}{\partial n} \tag{9}$$

where k is the electrolyte conductivity, and n is the unit vector.

2.4 Simulation method.

The simulation of the flow field and the electric field is shown in Figure 4. The three-dimensional model is first built with CATIA and then is imported into the simulation software

COMSOL Multiphysics. Then, various properties, including the conductivity, the density and the dielectric constants of the workpiece, the electrolyte and the cathode, are defined. In addition, it is necessary to add a reasonable physical model and assign the boundary conditions. Finally, the simulation is conducted after the mesh has been divided with the subdivision.

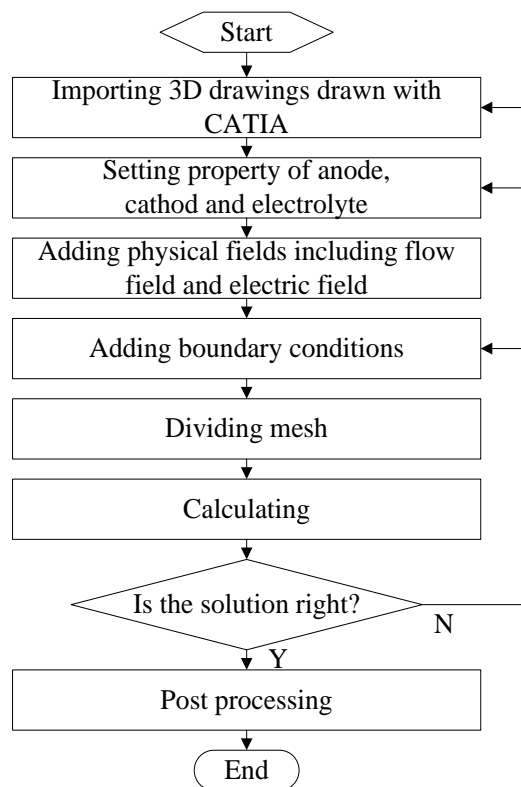


Figure 4. The flowchart of the simulation.

3. EXPERIMENTAL

3.1 Experimental setup

The experiments are carried out with the ECM system shown in Figure 5. The system consists mainly of a five-axis machine tool platform, a pulse power supply system, a control system, a numerical control system and an electrolyte circulation system. The machine tool can move in the X-, Y- and Z-directions and rotate around the X-axis and the Z-axis. The travels of the X-axis, the Y-axis and the Z-axis are 500 mm, respectively. The positioning accuracy can reach 0.01 mm (X-axis, Y-axis and Z-axis), and the rotary accuracies are 25" (around the X-axis and the Z-axis). The pulse power supply can be adjusted in the range of 0 ~ 30 V, and its peak output current is 3000 A. The control system is used to control the electrical parameters and the start-stop actions of the electrolyte pumps and the power switches and to display the running status. The FANUC Series Oi system serves to control the motions of the machine tool, the NC programming, etc. The electrolyte circulation system consists of an electrolyte pump, a filter, a solenoid valve, a pressure gauge and some pipes. The electrolyte is injected into the machining gap from the electrolyte tank and returns to the filtering tank

through pipelines. The electrolyte can be filtered to remove the impurities, and the electrolyte pressure can be controlled with the valve.

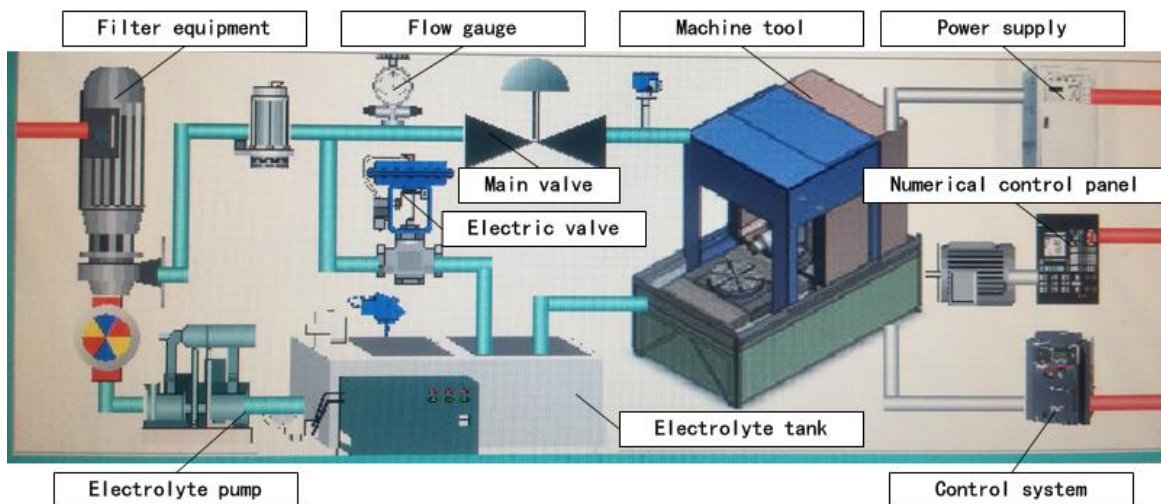


Figure 5. Schematic diagram of the ECM system.

3.2 Machining experiments

The machining principle diagram of the inner-walled ring groove is shown in Figure 6. The working surface of the cathode is modified into an inward curved surface with a small curvature value. The workpiece material is 1J116, and its chemical composition is shown in Table 1. Before machining the ring groove, a prefabricated hole with a diameter of 11.8 mm is machined on the workpiece.

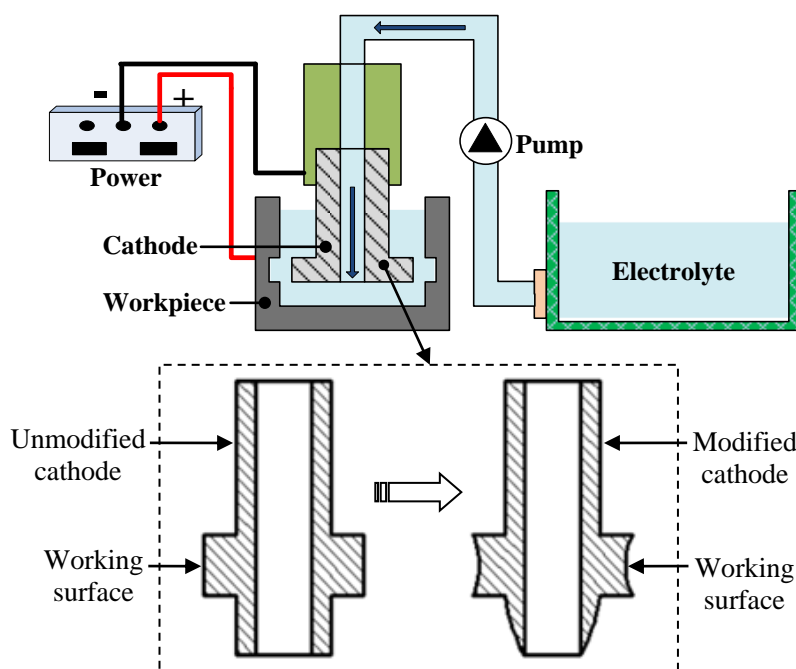


Figure 6. The machining principle diagram of the inner-walled groove.

During machining, the workpiece is linked with the positive pole of the pulse power supply,

and the cathode is linked with the negative pole. The electrolyte (10 wt % NaCl+16 wt % NaNO₃+2 wt % NaClO₃) is supplied from the end of the workpiece and passes through the machining area. The optimal experimental parameters are shown in Table 2. With the passing of time, the material at the machining area is dissolved into the electrolyte and taken away, and the inner-walled ring groove is formed.

Table 1. Chemical composition of 1J116.

Elements	C	P	S	Si	Mn	Al	Fe
Composition (wt %)	≤0.03	≤0.015	≤0.015	≤0.15	≤0.01	≤16.3	Remains

Table 2. The optimal experimental parameters.

Main parameters	Value
Machining voltage	14 V
Pulse frequency	500 Hz
Duty ratio	90 %
Machining gap	100 μm
Electrolyte	10 wt % NaCl + 16 wt % NaNO ₃ + 2 wt % NaClO ₃
Electrolyte temperature	29~31 °C
Inlet pressure	120 kPa
Machining time-length	180 s

4. RESULTS AND DISCUSSION

4.1 Simulation results and discussion

4.1.1 Flow field distribution

Figure 7 and Figure 8 show the flow field distribution when the curvature (ρ) of the working surface of the modified cathode equals 0.044 and 0.088, respectively. The curvature values of 0.044 and 0.088 are selected according to multiple simulation results and experimental results. As shown in the figures, whether the curvature is 0.044 or 0.088, the pressure fields in the machining gap are uniformly distributed, and the flow velocity in the middle section is slightly smaller than the flow velocity at both ends. Overall, the flow field distributions are better than the flow field distributions when the working surface of the cathode is not modified [12].

In ECM, the condition of the flow field is an important factor affecting the machining efficiency, accuracy and stability [20-22]. Zhu [23] found that a proper increase in the flow rate can effectively increase the electrolyte velocity and improve the flow field uniformity, and the flow velocity distribution has a good consistency with the processing depth.

When the working surface is modified into an inward curved surface with a small curvature radius, the machining gap in the middle section is slightly larger than the machining gaps at both ends, which makes the electrolyte velocity in the middle section a little slower than the electrolyte velocity at

both ends, as proved by Figure 7(a) and Figure 8(a). This lower electrolyte velocity is helpful to reduce the drum shape, to decrease the overcut amount in the middle section and to make the bottom of the groove flat. That is, the better-distributed flow field makes the bottom of the groove flatter than when the working surface of the cathode is not modified. Similarly, Fang [24] found the flow field distribution can affect the surface profile of the workpiece. Many other researchers also studied the effects of flow field distributions on surface profile and machining quality and achieved similar results [23, 25, 26].

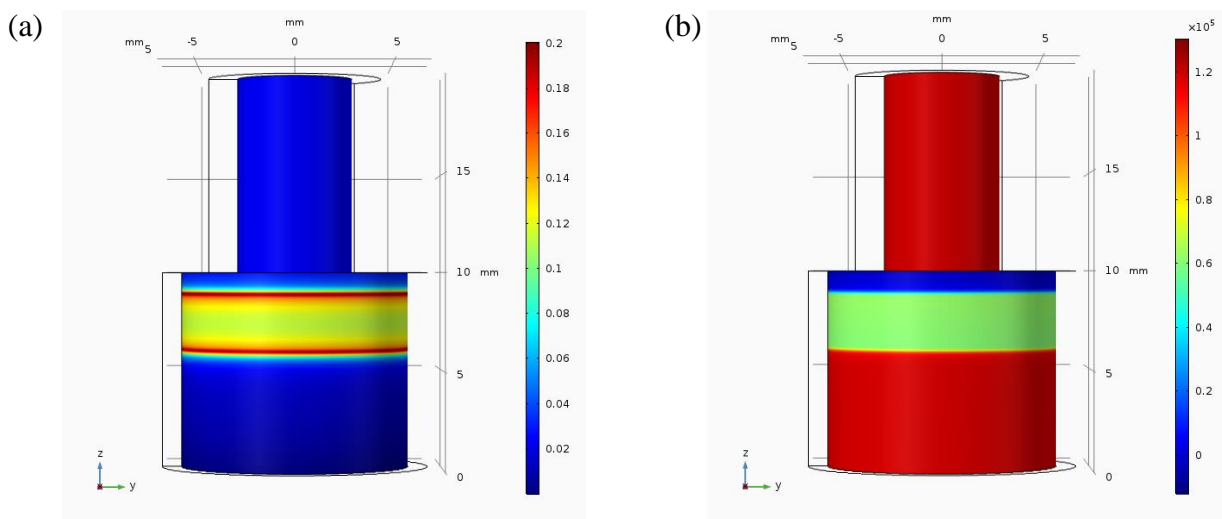


Figure 7. Flow field distribution ($\rho_1 = 0.044$): (a) velocity field (m/s) and (b) pressure field (Pa).

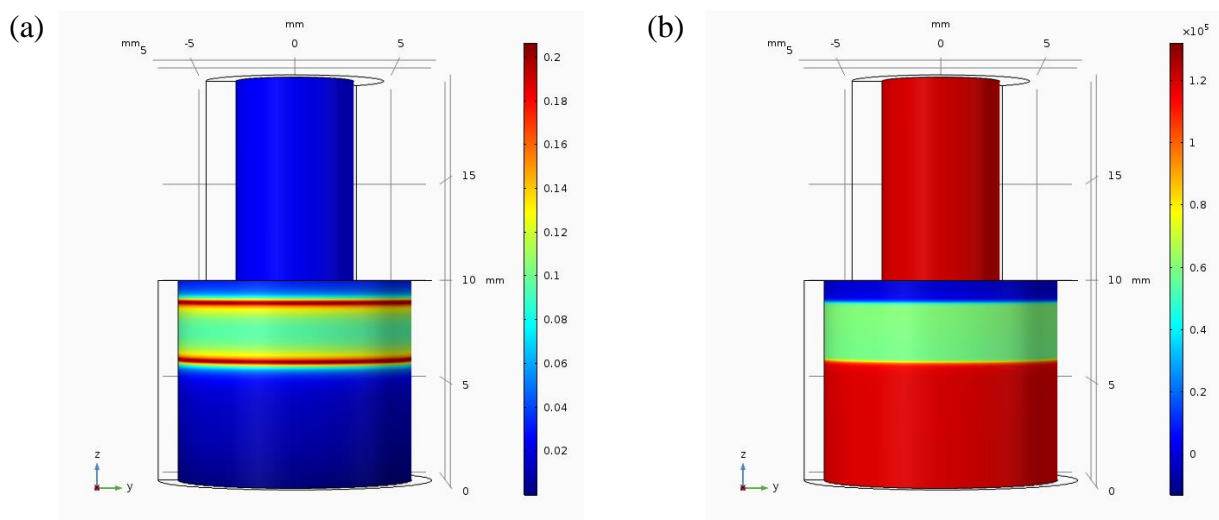


Figure 8. Flow field distribution ($\rho_2 = 0.088$): (a) velocity field (m/s) and (b) pressure field (Pa).

4.1.2 Electric field distribution

Figure 9 shows the electric field distribution when the curvature of the modified cathode surface equals 0.044. As Figure 9(b) shows, the minimum current density is approximately 16 A/cm², the maximum current density is 22 A/cm², and the current density in the middle section of the machining gap is slightly smaller than the current density at the two ends. As shown in Figure 9(f), the electric field intensity in the middle section is also slightly lower than the electric field intensity at the

two ends, and the maximum electric field intensity is 1.3 V/m. Similarly, Figure 10 shows the electric field distribution when the surface curvature equals 0.088. Figure 10(b) shows that the minimum current density is approximately 10 A/cm², the maximum current density is 15 A/cm², and the current density in the middle section is slightly smaller than the current density at the two ends.

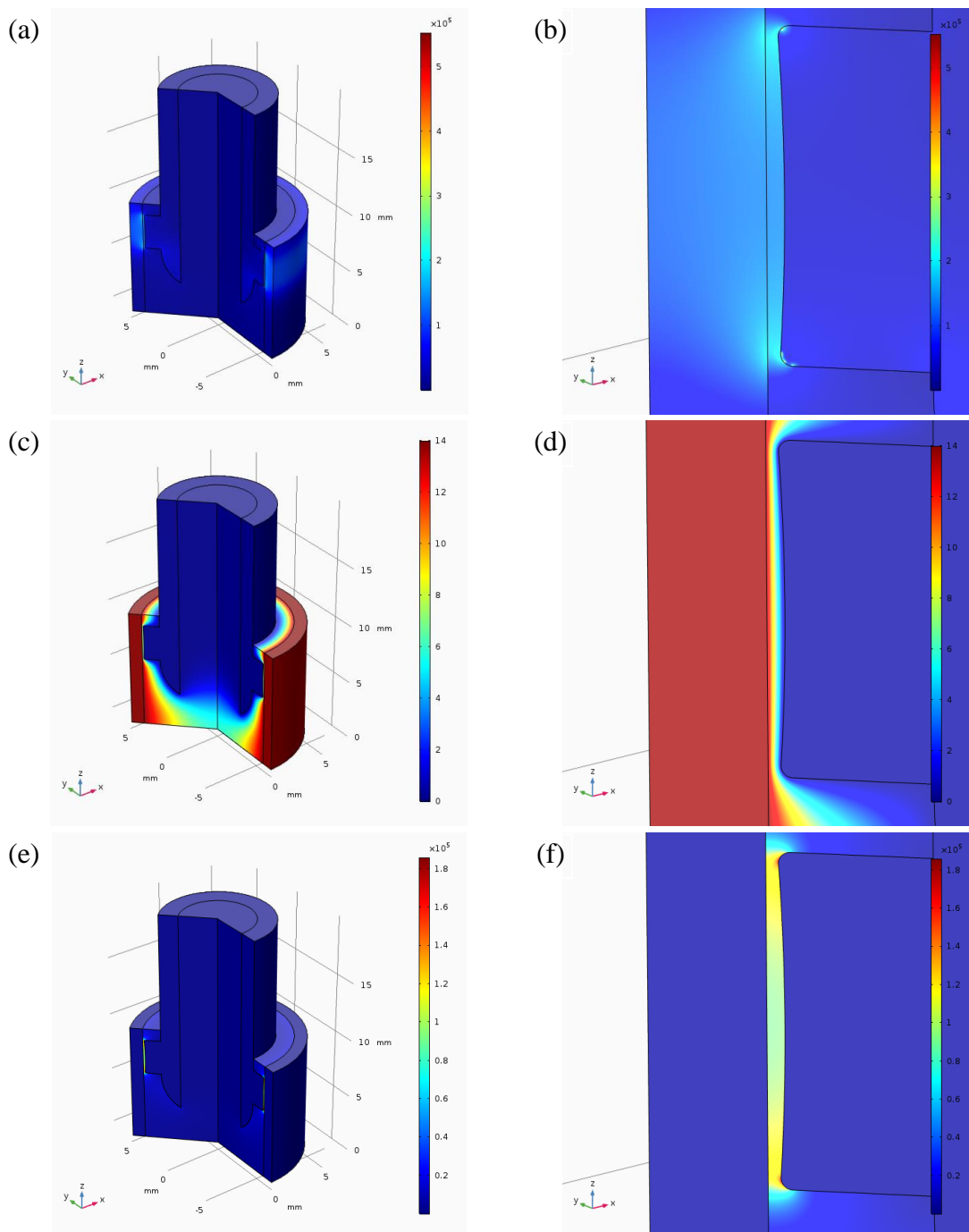


Figure 9. Electric field distribution ($\rho_1 = 0.044$): (a) current density (A/m²), (b) partial enlargement of the current density, (c) electric potential (V), (d) partial enlargement of the electric potential, (e) electric field intensity (V/m) and (f) partial enlargement of the electric field intensity.

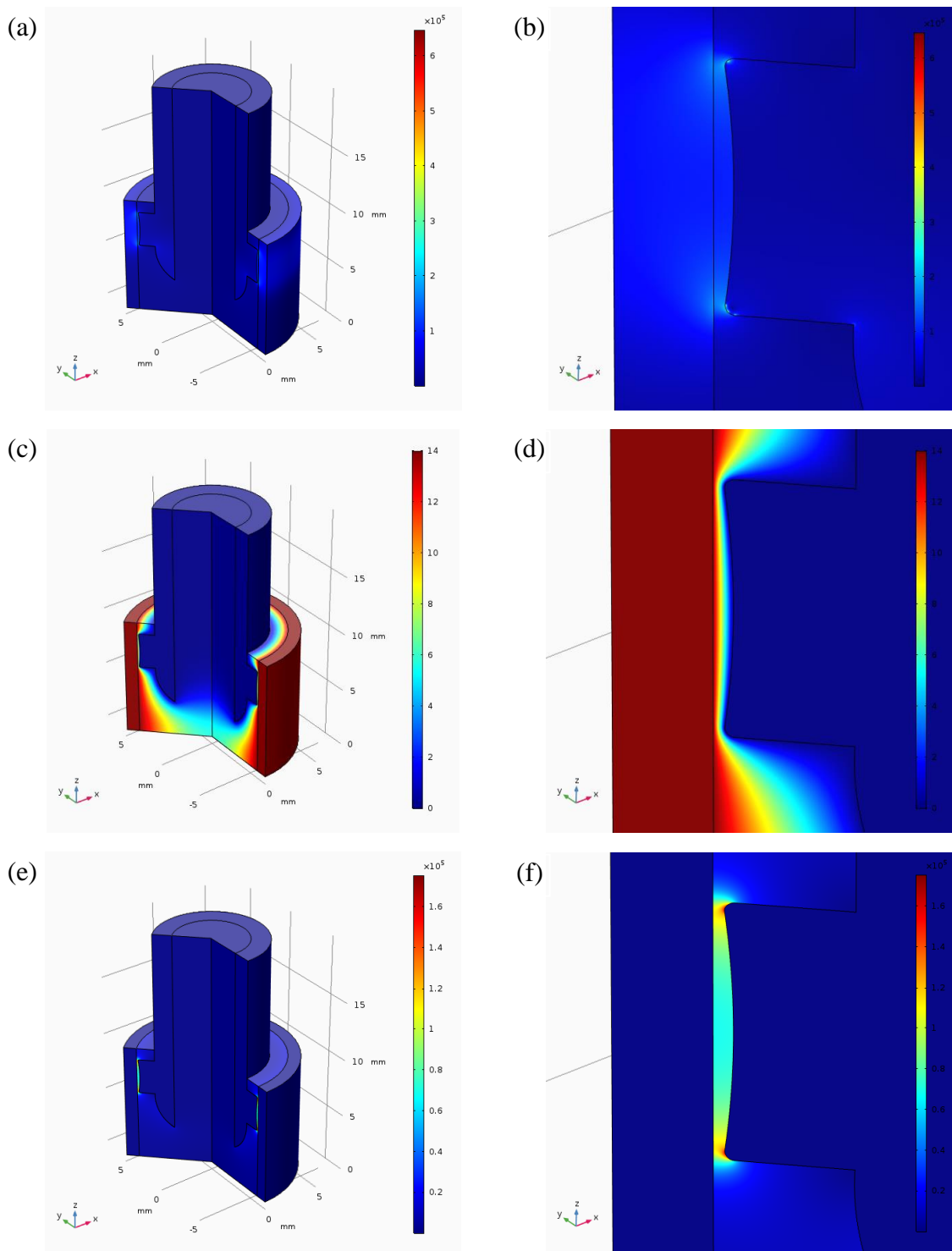


Figure 10. Electric field distribution ($\rho_2 = 0.088$): (a) current density (A/m^2), (b) partial enlargement of the current density, (c) electric potential (V), (d) partial enlargement of the electric potential, (e) electric field intensity (V/m) and (f) partial enlargement of the electric field intensity.

As shown in Figure 10(f), the electric field intensity in the middle section is also slightly lower than the electric field intensity at both ends, and the maximum electric field intensity is 1.1 V/m. Overall, the electric field distributions are better than the electric field distributions when the working surface of the cathode is not modified [12].

In ECM, the dissolution rate of the workpiece can be expressed as $v = \eta\omega i$. That is, the material removal rate v depends on the current density i . This conclusion has been proven by many studies. Sudiarso [27] concluded that there was a strong positive relationship between the material removal rate and the average steady current density after many experiments were conducted on various workpiece materials. Jin [28] and Nasir [29] drew the same conclusion. According to this theory and conclusion, when the working surface is modified into an inward curved surface with a small curvature radius, the machining gap in the middle section is slightly larger than the machining gaps at both ends, which makes the current density in the middle section also slightly smaller than the current density at both ends, as proven by Figure 9(b) and Figure 10(b). According to Faraday’s Law, the dissolution rate in the middle section is slightly smaller than the dissolution rates at both ends. This smaller dissolution rate is helpful to decrease the overcut amount in the middle section with the conventional cylindrical working surface cathode and to reduce the drum shape. The better-distributed electric field makes the bottom of the groove flatter than when the working surface of the cathode is not modified. Similarly, many researchers studied the effects of electric field distribution on surface profiles and achieved similar results [30-32].

4.1.3 Surface profile prediction

Figure 11 and Figure 12 are the surface profile prediction diagrams of the inner-walled ring grooves machined with two modified cathodes whose curvatures of the working-section surfaces equal 0.044 and 0.088, respectively. The surface profiles of different machining time-lengths are fitted according to the material removal rates and the amount removed at different locations based on the distribution of the current density. The depths of the ring groove in the middle section are slightly smaller than the depths of the ring groove at two ends.

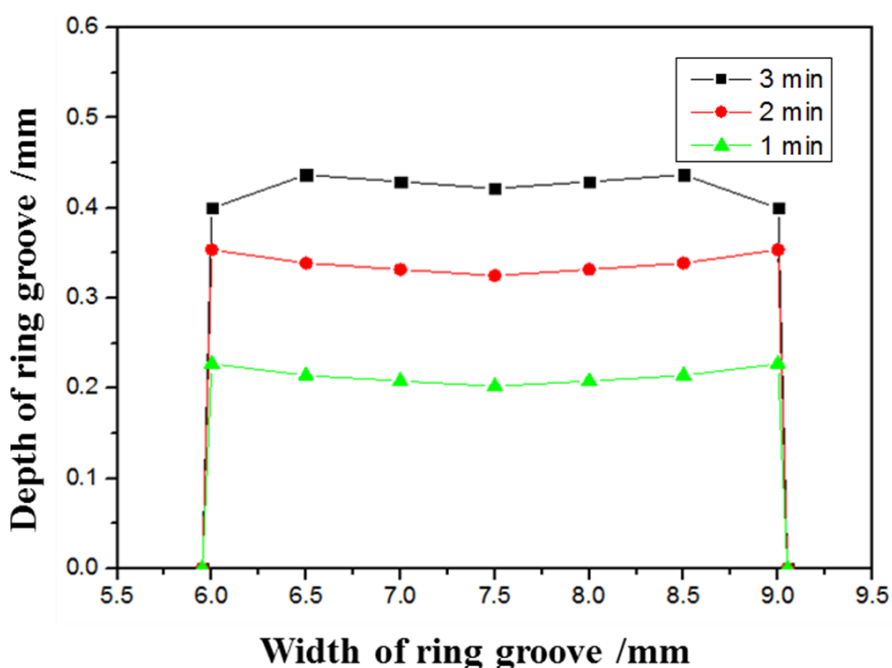


Figure 11. Surface profile prediction diagram ($\rho_1 = 0.044$).

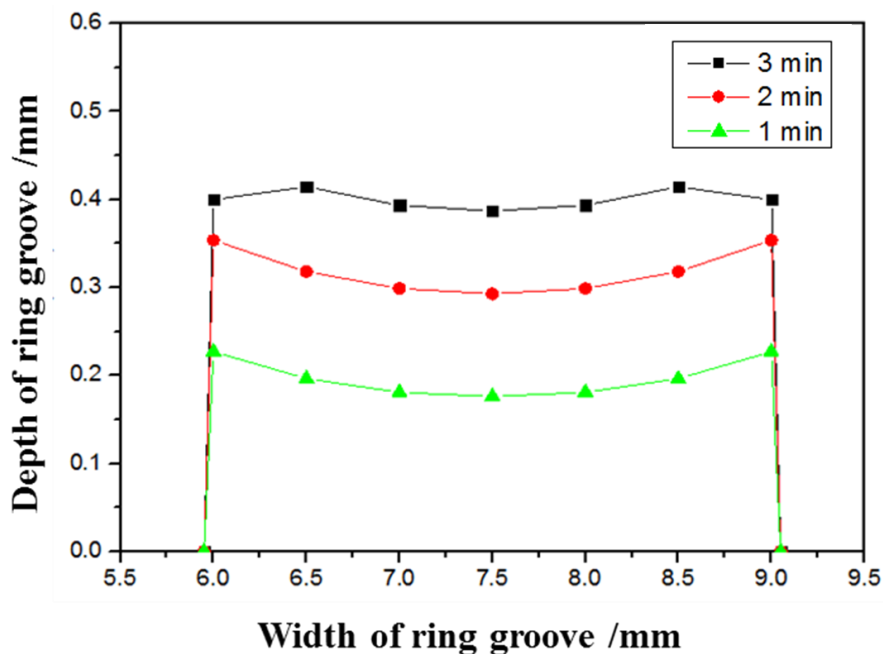


Figure 12. Surface profile prediction diagram ($\rho_2 = 0.088$).

In ECM, the relationship between the material removal rate v_a of the workpiece and the machining gap Δ can be expressed as $v_a = C/\Delta$, where C is a constant. When the working surface of the cathode is modified into an inward curved surface with a small curvature radius, the machining gap Δ in the middle section is slightly larger than the machining gaps at both ends, which can result in slightly lower material removal rate in the middle section. This lower removal rate is helpful to decrease the overcut amount in the middle section with the conventional cylindrical working surface cathode and to reduce the drum shape. The two figures are helpful for predicting the surface profiles of the machined grooves before actual machining and for selecting the curvature parameter of the working-section surface. Similar study methods can be seen in [26, 33, 34].

4.2 Experimental results and discussion

One of the machined inner-walled ring grooves with the modified cathode is shown in Figure 13, and its measurement results are shown in Figure 14. The machined groove is flat at the bottom and is not of a drum-shape. The machining quality of this groove is much better than those grooves machined with the conventional cylindrical working surface cathode (the unmodified cathode, see Figure 1).

Why can the machining quality of the groove be improved with the modified cathode? According to Faraday’s Law, the workpiece dissolution rate is determined by the current density. That is, decreasing the current density can decrease the material removal rate of the workpiece. The current density can be decreased by increasing the machining gap of the middle section of the machining gap when other parameters are kept unchangeable [35, 36]. This viewpoint can also be confirmed by the simulation results shown in Figure 9(b) and Figure 10(b). In addition, the modified inward curved surface makes the flow field distributions better than when the cathode is not modified, and the

electrolyte velocity in the middle section is slightly smaller than the electrolyte velocity at both ends. All these factors together decrease the overcut amount in the middle section with the conventional cylindrical cathode and reduce the drum shape.

The experimental results show that the proposed working surface-curvature modification method is feasible and effective for decreasing the overcut amount in the middle section and for reducing the drum shape. Simultaneously, modifying the working surface into an inward curved surface is a simple and convenient way to operate, which can easily be applied to other aspects.

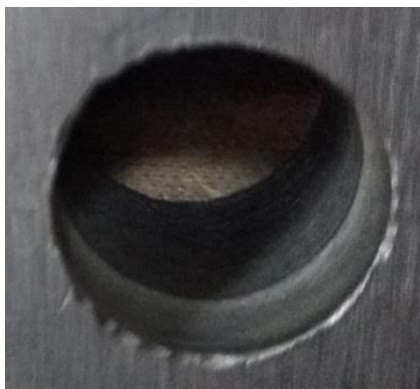


Figure 13. The machined groove (pulse frequency = 500 Hz, duration ratio = 90 %, machining voltage =14 V, machining gap =100 μm, electrolyte temperature = 30 °C, inlet pressure = 120 kPa and machining time-length = 180 s).

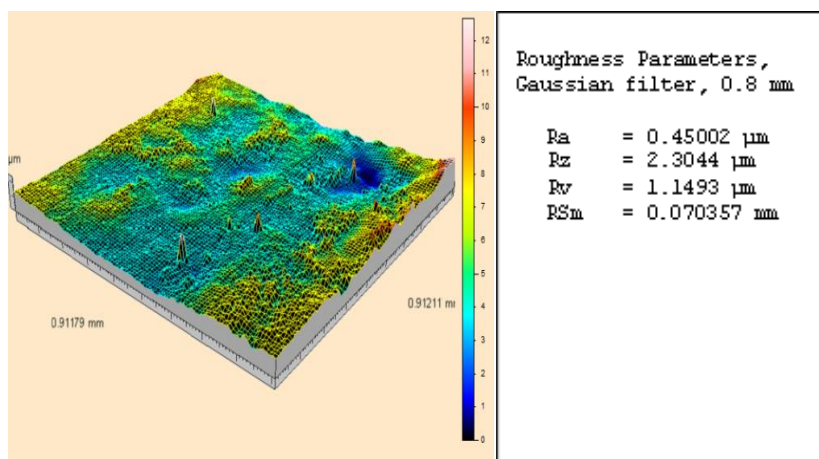


Figure 14. Surface morphology and roughness.

5. CONCLUSIONS

ECM is a promising and feasible machining technology for the inner-walled ring groove of the corrosion resistant alloy (1J116). The simulation results showed that the current density, the flow velocity of electrolyte and the material removal rate in the middle section decreased when the working surface was modified into an inward curved surface with a small curvature, which is helpful for decreasing the overcut amount in the middle section with the conventional cylindrical cathode and for

reducing the drum shape. The experimental results showed that the machined inner-walled ring groove was of good quality, and the bottom of the groove was flat. The experimental results agreed with the simulation results. This study is meaningful to provide a probable solution to improve the machining quality of the inner-walled structure workpieces without residual stress, recast layers or microcracks.

ACKNOWLEDGMENTS

This work was financially supported by the National Natural Science Foundation of China (No.51805404), the Projects of Science and Technology Department in Shaanxi Province (No. 2014JM2-5072, No. 2014SZS20-Z02 and No. 2014SZS20-P06) and the Projects of the Department of Education in Shaanxi Province (No. 13JS043 and No. 17JK0367).

References

1. R.J. Leese and A. Ivanov, *Adv. Mech. Eng.*, 8(2016)1.
2. M.M. Lohrengel, K.P. Rataj and T. Münnhoff, *Electrochim. Acta*, 201(2016)348.
3. K.P. Rajurkar, D. Zhu, J.A. Mcgeough, J. Kozak and A.D. Silva, *CIRP Ann. - Manuf. Techn.*, 48(1999)567.
4. Z.Y. Xu, Q. Xu, D. Zhu and T. Gong, *CIRP Ann. - Manuf. Techn.*, 62(2013)187.
5. G.M. Lin and H.Z. Cai, *Adv. Mat. Res.*, 472-475(2012)875.
6. D. Wang, Z. Zhu, N. Wang, D. Zhu and H. Wang, *Electrochimica. Acta*, 156(2015)301.
7. S. Langmaak, S. Wiseall, C. Bru, R. Adkins, J. Scanlan and A. Sóbester, *Int. J. Prod. Econ.*, 74(2013)142.
8. K.P. Rajurkar, M.M. Sundaram and A.P. Malshe, *Procedia. CIRP*, 6(2013)13.
9. X. Liu, X. Kang, W. Zhao and W. Liang, *Procedia. CIRP*, 6(2013)107.
10. G. Liu, Y. Li, Q. Kong and H. Tong, *Precis. Eng.*, 47(2017)508.
11. D. Mi and W. Natsu, *Precis. Eng.*, 42(2015)79.
12. C. Zhang, H. Ai, Z. Yan, X. Jiang, P. Cheng, Y. Hu and H. Tian, *Int. J. Adv. Manuf. Technol.*, 105(2019)4634.
13. J. Liu, Z. Fang, S. Deng and D. Zhu, *J. Nanjing Univ. Aeronaut. Astronaut.*, 46(2014)744.
14. L. Wang and D. Zhu, *Trans. Nonferrous Met. Soc. China*, 15(2005)241.
15. D. Zhu and Z.Y. Xu, *J. South China Univ. Techno.*, 38(2010)60.
16. Z. Xu, D. Zhu and D. Zhu, *J. Mech. Eng.*, 45(2009)187.
17. H. Li, S. Fu, S. Niu and N. Qu, *Int. J. Electrochem. Sci.*, 13(2018)6608.
18. Y. Liu, X. Xu, C. Guo and H. Kong, *Micromachines*, 10(2019)476.
19. G.Q. Wang, H.S. Li, N.S. Qu and D. Zhu, *J. Mater. Process. Tech.*, 234(2016)95.
20. J. Zhao, F. Wang, Z. Liu, X. Zhang, W. Gan and Z. Tian, *Chin. J. Aeronaut.*, 29(2016)1830.
21. D. Zhu and H.Y. Xu, *J. Mater. Process. Tech.*, 129(2009)15.
22. D. Deconinck, S.V. Damme, C. Albu, L. Hotoiu and J. Deconinck, *Electrochim. Acta*, 56(2011)5642.
23. D. Zhu, T. Xue, X. Hu and Z. Gu, *Chin. J. Aeronaut.*, 32(2019)1748.
24. X.L. Fang, N.S. Qu, Y.D. Zhang, Z.Y. Xu and D. Zhu, *J. Mater. Process. Technol.*, 214(2014)36.
25. L. Dabrowski and T. Paczkowski, *Russ. J. Electrochem.*, 41(2011)102.
26. D. Zhu, C. Liu, Z. Xu and J. Liu, *Chin. J. Aeronaut.*, 29(2016)1111.
27. A. Sudiarso, N.L.F. Ramdhani and M. Mahardika, *Int. J. Min. Metall. Mech. Eng.*, 1(2013)14.
28. D. Jin, K. Chu and E. Lee, *Chin. J. Aeronaut.*, 30(2017)1231.
29. K. Nasir, *Int. J. Res. Appl. Sci. Eng. Technol.*, 3(2015)35.
30. T. Kendall, P. Bartolo, D. Gillen and C. Diver, *Int. J. Adv. Manuf. Technol.*, 105(2019)651.

31. H. Hocheng, Y.H. Sun, S.C. Lin and P.S. Kao, *J. Mater. Process. Tech.*, 140(2003)264.
32. Z. Wang, S. Qian, H. Cao, H. Zhang and K. Bao, *Int. J. Electrochem. Sci.*, 11(2016)6126.
33. Y. Zhu, J. Xu and P. Hu, *Chin. J. Aeronaut.*, 14(2001)376.
34. J. Wu and J. Xu, *J. Syst. Simul.*, 21(2009)73.
35. A.B. Kamaraj and M. Sundaram, *J. Appl. Electrochem.*, 48(2018)463.
36. E.L. Hotoiu, S.V. Damme, C. Albu, D. Deconinck, A. Demeter and J. Deconinck, *Electrochim. Acta*, 93(2013)8.

© 2020 The Authors. Published by ESG (www.electrochemsci.org). This article is an open access article distributed under the terms and conditions of the Creative Commons Attribution license (<http://creativecommons.org/licenses/by/4.0/>).